Aneurysm Wall Enhancement Is Associated With Decreased Intrasaccular IL-10 and Morphological Features of Instability

Vanessa M. Swiatek, cand. med.[‡*]
Belal Neyazi, MD[‡*]
Jorge A. Roa, MD[§¶]
Mario Zanaty, MD[§]
Edgar A. Samaniego, MD, MS[§¶]
Daizo Ishii, MD[§]
Yongjun Lu, PhD[§]
I. Erol Sandalcioglu, MD[‡]
Sylvia Saalfeld, PhD[‖#]
Philipp Berg, PhD[#**]
David M. Hasan, MD[§]

[‡]Deparment of Neurosurgery, Otto-von-Guericke University, Magdeburg, Saxony Anhalt, Germany; [§]Deparment of Neurosurgery, University of Iowa Hospitals and Clinics, Iowa City, Iowa, USA; [¶]Deparment of Neurology, University of Iowa Hospitals and Clinics, Iowa City, Iowa, USA; [‖]Deparment of Simulation and Graphics, University of Magdeburg, Magdeburg, Saxony Anhalt, Germany; [#]Research Campus STIMULATE, Magdeburg, Saxony Anhalt, Germany; [**]Department of Fluid Dynamics and Technical Flows, University of Magdeburg, Magdeburg, Saxony Anhalt, Germany

*Vanessa M. Swiatek and Belal Neyazi contributed equally to this work.

Correspondence:
David M. Hasan, MD,
Department of Neurosurgery,
University of Iowa Hospitals and Clinics,
200 Hawkins Dr,
Iowa City, IA 52242, USA.
Email: david-hasan@uiowa.edu

Received, October 17, 2020.
Accepted, May 8, 2021.
Published Online, July 9, 2021.

BACKGROUND: High-resolution vessel wall imaging plays an increasingly important role in assessing the risk of aneurysm rupture.

OBJECTIVE: To introduce an approach toward the validation of the wall enhancement as a direct surrogate parameter for aneurysm stability.

METHODS: A total of 19 patients harboring 22 incidental intracranial aneurysms were enrolled in this study. The aneurysms were dichotomized according to their aneurysm-to-pituitary stalk contrast ratio using a cutoff value of 0.5 (nonenhancing < 0.5; enhancing ≥ 0.5). We evaluated the association of aneurysm wall enhancement with morphological characteristics, hemodynamic features, and inflammatory chemokines directly measured inside the aneurysm.

RESULTS: Differences in plasma concentration of chemokines and inflammatory molecules, morphological, and hemodynamic parameters were analyzed using the Welch test or Mann-Whitney *U* test. The concentration ΔIL-10 in the lumen of intracranial aneurysms with low wall enhancement was significantly increased compared to aneurysms with strong aneurysm wall enhancement ($P = .014$). The analysis of morphological and hemodynamic parameters showed significantly increased values for aneurysm volume ($P = .03$), aneurysm area ($P = .044$), maximal diameter ($P = .049$), and nonsphericity index ($P = .021$) for intracranial aneurysms with strong aneurysm wall enhancement. None of the hemodynamic parameters reached statistical significance; however, the total viscous shear force computed over the region of low wall shear stress showed a strong tendency toward significance ($P = .053$).

CONCLUSION: Aneurysmal wall enhancement shows strong associations with decreased intrasaccular IL-10 and established morphological indicators of aneurysm instability.

KEY WORDS: Hemodynamics, Inflammation, Intracranial aneurysm, Magnetic resonance imaging, Morphology, Wall enhancement

Neurosurgery 89:664–671, 2021 https://doi.org/10.1093/neuros/nyab249 www.neurosurgery-online.com

Unruptured intracranial aneurysms (UIAs) are often diagnosed incidentally in the context of noninvasive neuroimaging, and occur in 3% to 5% of the adult population worldwide.[1,2] Early identification of UIAs with high rupture risk is necessary for best patient care in neurosurgical daily practice.

An increasing number of centers focus on investigating the role of high-resolution vessel wall imaging (HR-VWI) on the rupture risk of intracranial aneurysms (IAs), but no standardized method is established so far. Nevertheless, aneurysm wall enhancement (AWE) is known to be associated with inflammation, aneurysm growth, and rupture[3,4]; strong AWE is therefore interpreted as a biomarker of aneurysminstability. To date, no study has

ABBREVIATIONS: **AWE,** aneurysm wall enhancement; **CE-MRA,** contrast-enhanced magnetic resonance angiography; **FSE,** fast-spin-echo; **HR-VWI,** high-resolution vessel wall imaging; **IA,** intracranial aneurysm; **IM,** inflammatory mediator; **MCP-1,** monocyte chemoattractant protein-1; **NSI,** nonsphericity index; **OSI,** oscillatory shear index; **SI,** signal intensity; **WSS,** wall shear stress

Supplemental digital content is available for this article at www.neurosurgery-online.com.

TABLE 1. Patient's Characteristics

Patient Nr.	Age	Sex	CR_{stalk}	Aneurysm size (in mm)	Localization	Embolization procedure
1	63	M	0.58	6	R. MCA	WEB device
2	65	M	1.07	7	R. ICA	WEB device
3	55	F	0.52	3	R. ACA	Coiling
4	77	F	0.72	8	Basilar tip	WEB device
5	36	F	0.58	6	R. ICA	Pipeline
			0.46	4	R. ICA	Pipeline
			0.69	3	L. ICA	Coiling
6	38	F	0.52	3	R. ICA	Coiling
7	86	F	0.39	5	Acom	WEB device
8	47	F	0.83	10	L. Pcom	Coiling
9	79	F	0.63	7	L. ICA	WEB device
10	74	F	0.47	5	Acom	WEB device
11	88	M	0.97	9	Acom	Coiling
12	59	F	0.32	3	Basilar tip	Coiling
13	64	M	0.61	3	Acom	Coiling
14	55	F	0.78	5	R. ICA	Pipeline
15	59	F	0.59	3	L. ICA	Pipeline
16	69	F	0.37	4	L. ICA	Pipeline
17	69	F	0.66	10	L. ICA	WEB device
			0.48	5	L. MCA	WEB device
18	75	F	0.42	4	L. VA	Coiling
19	66	F	0.33	5	R. MCA	WEB device

M, male; F, female; CRstalk, aneurysm-to-pituitary stalk contrast ratio; R, right; L, left; ICA, internal carotid artery; ACA, anterior cerebral artery; Acom, anterior communicating artery; MCA, middle cerebral artery; Pcom, posterior communicating artery; VA, vertebral artery; WEB, Woven EndoBridge.

investigated the direct relationship between AWE, inflammatory mediators (IMs), and established morphological and hemodynamic risk factors for aneurysm rupture within the same patient. The most accurate way to establish AWE as a tool in the daily clinical assessment of aneurysm rupture risk would be a prospective study; on the other hand, prospective studies in patients with UIA remain subject to high ethical standards and, therefore, exclude a large number of patients. Therefore, we evaluated the association of AWE on HR-VWI with morphology, hemodynamics, and IMs directly measured inside the IA to introduce a first approach toward the validation of the AWE as a direct surrogate parameter for aneurysm stability.

METHODS

Patient Selection

This study protocol adheres to the strengthening the reporting of observational studies in epidemiology guidelines. A total of 19 patients harboring 22 intracranial saccular aneurysms were enrolled (Table 1). All patients presented to the Department of Neurosurgery at the University of Iowa Hospitals and Clinics and had their IA diagnosed incidentally. Our inclusion criteria were the following: presence of saccular UIA, feasibility of intrasaccular and internal carotid artery sampling via an endovascular approach, and no contraindications to undergo HR-VWI in a 3T magnetic resonance imaging (MRI) scanner. All patients underwent endovascular treatment via coiling or the use of a Woven EndoBridge device. The study protocol was conducted in compliance with the Declaration of Helsinki and approved by the University of Iowa Institutional Review Board. In addition, patient consent for participation and publication was obtained. The investigators of this study were not blinded to the rupture status of the IA.

HR-VWI Assessment

In this study, we used our previously published HR-VWI protocol,[5] which was acquired using a 3T Siemens MRI scanner (MAGNETOM Skyra, Siemens). The HR-VWI protocol included a 3D T1-weighted SPACE fast-spin-echo (FSE) sequence, a 3D T2-weighted sequence, as well as a postcontrast 3D T1-weighted SPACE FSE sequence and a contrast-enhanced magnetic resonance angiography (CE-MRA). The postcontrast 3D T1-weighted SPACE FSE sequence and CE-MRA were obtained 5 min after intravenous injection of 0.1 mmol/kg gadolinium-based contrast agent (Gadavist, Bayer Pharmaceuticals).

The protocol used in this study for assessment of AWE on HR-VWI has been previously described in the literature.[6,7] Briefly, the extracted pre- and postcontrast T1 sequences were manually co-registered in all 3 planes. The aneurysmal wall was delineated by drawing a 2D region of interest at the level of maximal aneurysm diameter. Contrast enhancement was quantified using the aneurysm-to-pituitary stalk contrast ratio (CR_{stalk}).[8] For the determination of the CR_{stalk}, the postcontrast T1-weighted images were analyzed according to Roa et al,[6] and the maximal signal intensity (SI) of the aneurysm wall was divided by the maximal SI of all sampled points over the pituitary stalk. The measurement of the AWE was performed by 2 independent experts. The agreement rate was 88% when dichotomizing the IAs into 2 groups according to a CR_{stalk} cutoff of 0.5.

Blood Sampling

All patients received 325 mg aspirin and 75 mg clopidogrel daily for 7 d prior to surgery; 3000 international units of intravenous heparin were applied intraoperatively. This medication regimen was used equally in every patient. The technique applied for intra-aneurysmal blood sampling has been previously described.[9-11] A 7-French sheath was inserted, and a guiding catheter was navigated into the target vessel. First, a 3-mL blood sample was collected from the ipsilateral parent artery as a control; a microcatheter was advanced over a micro guidewire and positioned inside the aneurysmal sac in close proximity to the inner wall of the dome. In this position, a second 3-mL blood sample was carefully drawn before endovascular treatment.

Blood samples were centrifuged at 1000 rpm for 15 min at 4°C, the plasma was aliquoted into small volumes (~200 μL), and immediately stored at –80°C until analysis. The plasma concentration of 27 different cytokines, chemokines, and growth factors was quantified with the Luminex-based immunoassay by using Bio-Plex Pro Human Cytokine 27-plex Assay (Cat #M500KCAF0Y, Bio-Rad Laboratories Inc, Hercules, California). This analysis included the following molecules: IL-1β, IL-1 receptor antagonist, IL-2, IL-4, IL-5, IL-6, IL-7, IL-8, IL-9, IL-10, IL-12, IL-13, IL-15, IL-17, eotaxin, basic fibroblast growth factor, granulocyte colony-stimulating factor, granulocyte monocyte colony-stimulating factor, IFN-γ, interferon-γ-induced protein-10 (IP-10), monocyte chemoattractant protein-1 (MCP-1), macrophage inflammatory protein-1-α, macrophage inflammatory protein-1-β, platelet-derived growth factor subunit B, normal T-cell-expressed and -secreted (RANTES), TNF-α, and vascular endothelial growth factor.

Morphology and Hemodynamics

We extracted a 3D surface model in accordance with Saalfeld et al[12,13] using 3D rotational-angiography and magnetic resonance angiography datasets. For morphological analysis, we applied a semiautomatic approach, which allows the automatic determination of 21 parameters based on the reconstruction of the neck curve[14] (Table 2). Additionally, we performed highly resolved, time-dependent blood flow simulations based on the patient's individual 3D surface model using computational fluid dynamics.[15] The results were assessed by 4 different examiners (2 neurosurgeons and 2 computer scientists) with extensive experience in this field.

Because no patient-specific boundary conditions were available, reasonable assumptions were made. Blood was treated as an incompressible fluid (1055 kg/m^3) with constant Newtonian viscosity (4 mPa*s); the blood flow was presumed to be laminar. Flow rates from a healthy volunteer were acquired using 7T phase-contrast MRI and applied at the inlet openings according to the individual cross-section.[16] Furthermore, an advanced outflow splitting model was used to determine the flow rates at the outlet openings,[17] whereas the vessel walls were assumed to be rigid. For each case, the simulation of 3 cardiac cycles was performed. Based on the last cardiac cycle simulation, 24 hemodynamic parameters were calculated[18] (Table 2).

HR-VWI, cerebral angiography, and morphological and hemodynamic assessment of an illustrational case are presented in Figure 1.

Statistics

The UIAs were dichotomized according to their CR_{stalk} using a cutoff value of 0.5 (nonenhancing < 0.5; enhancing ≥ 0.5). Using aneurysm size and location as clinical parameters of rupture risk, a CR_{stalk} cutoff of 0.6 was previously established by our group.[6] However, an internal validation study using presence of microbleeds in quantitative susceptibility mapping imaging as gold standard showed that the most accurate CR_{stalk} cutoff to predict aneurysm instability was 0.5. Using this cutoff, 8 IAs were classified as nonenhancing and 14 IAs as enhancing. Intrasaccular blood samples and control samples from the internal carotid artery were available for 17 out of 22 enrolled IAs; morphological and hemodynamic analysis was performed successfully for 21 out of 22 enrolled IAs. In order to analyze the differences in plasma concentration of IM between the IA and the control sample withdraw from the internal carotid artery, the concentrations of the control sample were subtracted from the intrasaccular concentration ($C_{aneurysm} - C_{control} = \Delta C$). The morphological and hemodynamic parameters were analyzed using the extracted absolute values. All variables were tested for normality of the distribution using the Kolmogorov-Smirnov test and analyzed using the parametric Welch test or the nonparametric Mann-Whitney U test. The results were considered statistically significant if they reached a P-value of $\leq$.05.

The absolute values of the measured morphological and hemodynamic parameters and IMs are available in **Table**, **Supplemental Digital Content**.

RESULTS

Of the 19 included patients, 4 patients were male, and 15 patients were female. The mean age was 64.4 yr (range: 36-88 yr). Mean aneurysm size was 5.4 (±2.3) mm. Detailed information on the characteristics of the patients is presented in Table 1.

Inflammation

The analysis of ΔC of IMs between the IA and the control sample revealed significantly increased ΔIL-10 in the lumen of UIAs with low AWE compared to IAs with strong AWE ($P = .014$). There was no difference in ΔC of the remaining IMs.

Morphology and Hemodynamics

The analysis of morphological and hemodynamic parameters showed significantly increased values for 4 out of 49 parameters, namely aneurysm volume ($P = .03$), aneurysm area ($P = .044$), maximal diameter (D max) ($P = .049$), and nonsphericity index (NSI) ($P = .021$) for UIAs with strong AWE. None of the hemodynamic parameters reached statistical significance, but the total viscous shear force computed over the region of low wall shear stress (F low) showed a tendency toward significance with AWE ($P = .053$). Regarding the hemodynamically relevant parameters time-averaged wall shear stress (WSS) and the oscillatory shear index (OSI), it was found that lower shear occurred in the enhancing group compared to the none-enhancing one (3.638 ± 2.676 Pa vs 6.888 ± 6.697 Pa). Furthermore, increased spatially averaged OSI (0.024 ± 0.045 vs 0.009 ± 0.007) was present in IAs with higher CR_{stalk}. Finally, the median values of the low shear areas—the part of the aneurysms that is subjected to abnormally low WSS—were considerable larger in enhancing cases (50.032% vs 21.495%) (Figure 2).

TABLE 2. Abbreviations and Definitions of 45 Morphological and Hemodynamic Parameters

Parameter	Definition
Morphological parameters	
H max	Maximum height of the aneurysm
W max	Maximum width perpendicular to H max
D max	Maximum diameter of the aneurysm
H ortho	Height of the aneurysm, measured vertically to the aneurysm neck
W ortho	Maximum width perpendicular to H ortho
N max	Maximum diameter of the aneurysm neck
N avg	Average diameter of the aneurysm neck
Aspect ratio 1 (AR 1)	H ortho/N max
Aspect ratio 2 (AR 2)	H ortho/N avg
Ellipticity index (EI)	$1 - 18^{(1/3)}$ VCH$^{(2/3)}$/ACH
Nonsphericity index (NSI)	$1 - 18^{(1/3)}$ volume$^{(2/3)}$/aneurysm area
Undulation index (UI)	1 – volume/VCH
Aneurysm area	Surface area of the aneurysm
Ostium area 1	Area of the aneurysm ostium
Ostium area 2	Area of the aneurysm ostium with the neck curve projected onto a plane
Volume	Volume of the aneurysm
VCH	Volume of the convex hull of the aneurysm
ACH	Surface area of the convex hull of the aneurysm
Alpha	Angle at B1 describing angle from base line to the dome point
Beta	Angle at B2 describing angle from base line to the dome point
Gamma	Angle on the aneurysm dome depending on base points
Mean neck in-flow rate	Neck flow rate averaged over one cardiac cycle
Hemodynamic parameters	
Q vessel	Flow rate within the parent vessel
Q vessel mean	Mean flow rate within the parent vessel
F aneurysm	Shear stress of the aneurysm area
F high	Shear stress of the aneurysm area under high wall shear stress
F low	Shear stress of the aneurysm area under low wall shear stress
Aneurysm AWSS mean	Mean average wall shear stress of the aneurysm
Aneurysm AWSS max	Maximal average wall shear stress of the aneurysm
A high	Area of the aneurysm under high wall shear stress
A low	Area of the aneurysm under low wall shear stress
Mean AWSS vessel	Mean average wall shear stress of the parent vessel
Variance AWSS vessel	Variance of the wall shear stress of the parent vessel
sdAWSS vessel	Standard deviation of average wall shear stress occurring on the parent vessel
AWSS vessel high	Abnormally high average wall shear stress on the parent vessel
AWSS vessel low	Abnormally low average wall shear stress on the parent vessel
Aneurysm OSI mean	Mean oscillatory shear index of the aneurysm
Aneurysm OSI max	Maximal oscillatory shear index of the aneurysm
Aneurysm RRT mean	Mean relative residence time of the aneurysm
Aneurysm RRT max	Maximal relative residence time of the aneurysm
ICI mean	Mean inflow concentration index
SCI	Shear concentration index
HSI	High shear index
LSI	Low shear index
LSA	Low shear stress area percentage

DISCUSSION

Key Results

We found a significantly increased difference in plasma concentration of IL-10 in IA with low AWE. Enhancing IAs were larger and showed significantly higher values for aneurysm volume, aneurysm area, and D max. In addition, nonenhancing UIAs more often showed irregular shape.

Interpretation

To date, no study has evaluated the direct association between AWE and in Vivo aneurysmal inflammation. Inflammation and immune system responses within aneurysm walls present a significant research field in researching the natural course of IA. Many studies reported increased occurrence of complement, immunoglobulins, and inflammatory cells in

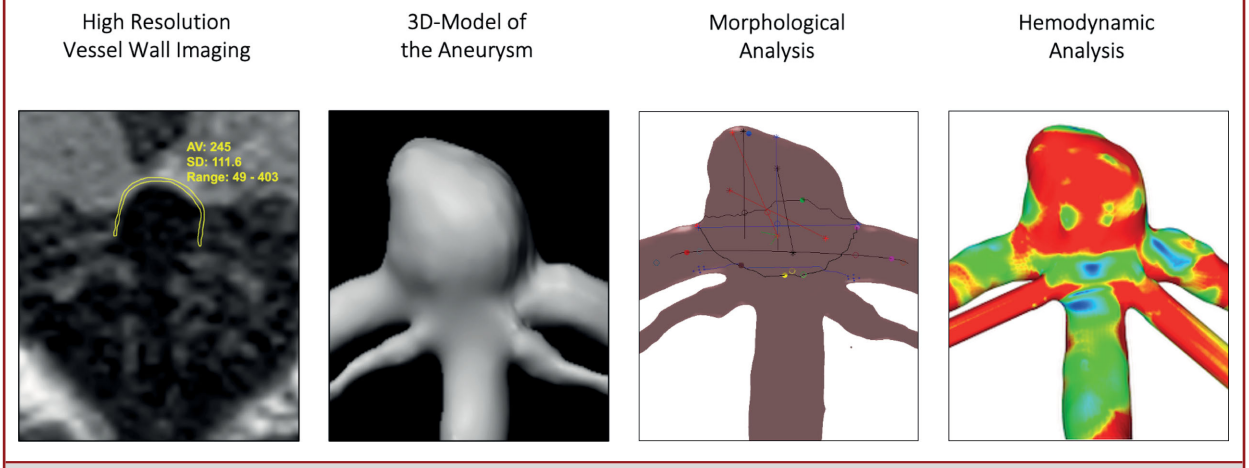

FIGURE 1. *HR-VWI, cerebral angiography, and morphological and hemodynamic assessment of an illustrational case (case 4). HR-VWI of a basilar tip aneurysm showing the methodology to quantify enhancement in the aneurysm wall. The workflow for the semiautomatic morphological and the hemodynamic analysis includes the extraction of a 3D model of the posterior circulation and the basilar tip aneurysm based on individuals neuroimaging. Both morphological and hemodynamic analyses can be visualized afterwards. Here, we show an exemplary screenshot from the semiautomatic neck reconstruction and an illustration of the AWSS (red color indicates high AWSS; blue color indicates low AWSS) as a result of computational fluid dynamics. HR-VWI, high-resolution vessel wall imaging; AWSS, average wall shear stress of the aneurysm.*

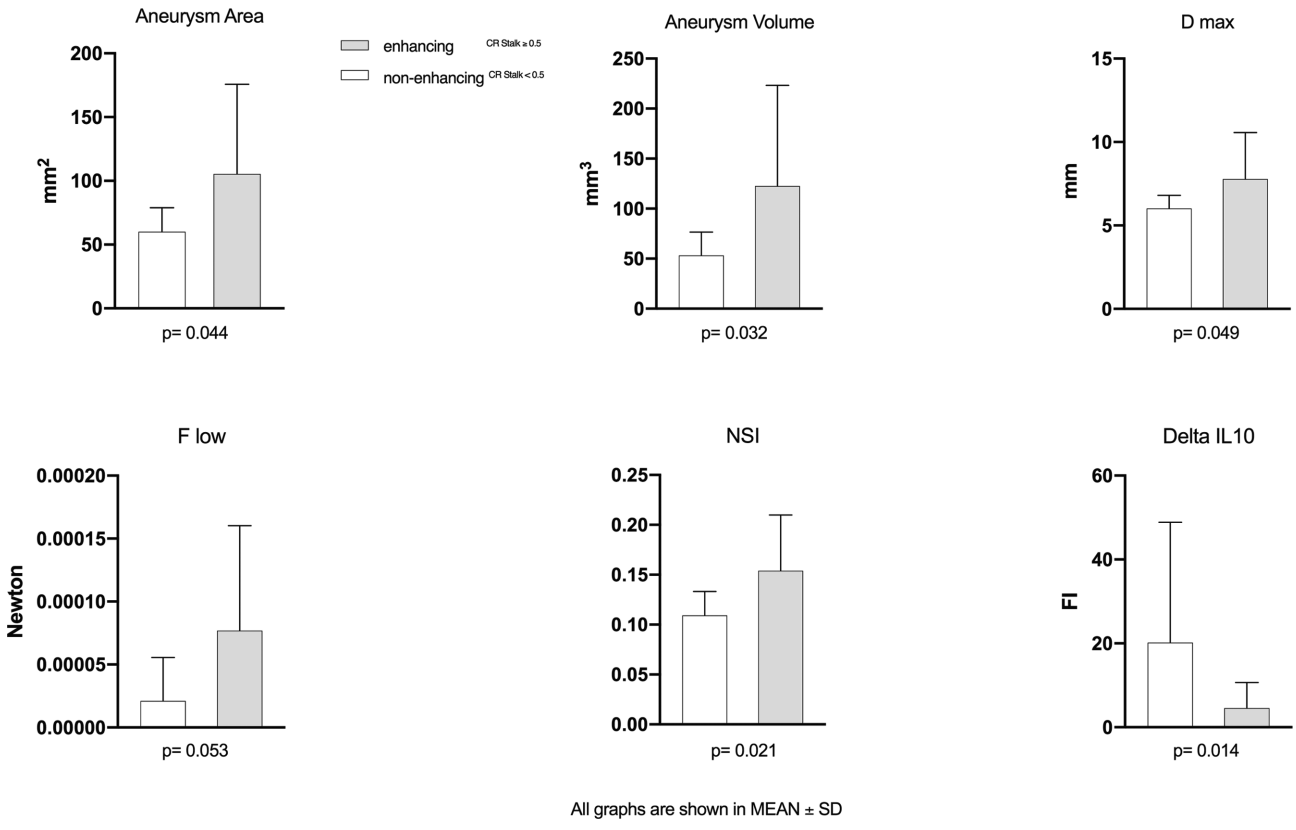

FIGURE 2. *Illustration of the mean values and the standard deviations for aneurysm area, aneurysm volume, D max, NSI, F low, and ΔIL-10. D max, maximum diameter of the aneurysm; NSI, nonsphericity index; F low, shear stress of the aneurysm area under low wall shear stress; ΔIL-10, differences in plasma concentration of IL-10.*

aneurysm walls[19-22]; infiltration of the aneurysm wall by cells of the immune system is associated with degeneration of the wall structure and aneurysm rupture.[19,23-25] Investigating the recruitment of inflammatory cells by chemokines and the mediation of inflammation via cytokines and other IMs in more detail could provide information about the pathogenesis of IA on the one hand and offer a possible therapeutic target on the other.[9,26-29] A previously published study of our group was the first study to address the concentration of IMs within the lumen of IA. It showed increased absolute plasma concentrations of RANTES, MIG, IL-10, eotaxin, IL-8, and IL-17 in the lumen of IA compared to peripherally collected blood samples from the femoral artery, whereas the plasma concentration of IL-6 was lower. When ruptured IAs were excluded from the analysis, increased absolute plasma concentrations were detected for MCP-1, RANTES, monokine induced by γ-interferon, IP-10, eotaxin, IL-8, and IL-17.[9] All these molecules have inflammatory effects and play an important role in the chemotaxis of macrophages, T cells, eosinophils, basophils, and neutrophils.[26,30] In this study, we focused on the association of AWE and associated differences in plasma concentrations of inflammatory molecules and chemokines between enhancing and nonenhancing IA. We found a significantly increased difference in plasma concentration of IL-10 in IA with low AWE. IL-10 is an anti-inflammatory cytokine. IL-10 inhibits the production of proinflammatory molecules like IFN-γ, IL-2, IL-4, IL-5, IL-1β, IL-6, IL-8, IL-12, and TNF-α by different cells of the immune system.[30] Therefore, a deficiency of IL-10 is associated with prolonged immune response, excessive inflammation, and tissue damage; an increased secretion of IL-10 seems to suppress inflammatory processes. In the context of arteriosclerosis, regulatory T cells and their secretion of anti-inflammatory cytokines such as IL-10 has already been studied in detail and was identified as an important biomarker and possible therapeutic target.[31] Some studies have demonstrated the vasoprotective effect of an increased secretion of IL-10 in the pathogenesis of arteriosclerosis.[32,33] Therefore, our results suggest that the inflammation in aneurysm walls might be T cell modulated. Overall, these findings support our hypothesis that an increased concentration of IL-10 in IAs with low AWE may represent stability.

Previous studies already described an association between well-established morphological predictors of aneurysm rupture (larger aneurysm size[3,34,35] and irregular aneurysm shape[3,36]) with increased AWE. Size-related parameters and irregularity indices of UIAs have been extensively researched and are strongly associated with their rupture.[37-41] In our study, enhancing IAs were larger and showed significantly higher values for some size-related morphological parameters: aneurysm volume, aneurysm area, and D max. In addition, nonenhancing UIAs more often showed irregular shape and increased deviation of the surface geometry from that of a perfect hemisphere, which is described by the NSI.[41] Aneurysm morphology and flow conditions interact with each other and are closely related.[42,43] Among all the measurements obtained by computational fluid dynamics, the most promising parameter seems to be WSS. Although it is unclear whether high WSS, low WSS, or both induce aneurysm growth and rupture,[44] it can be assumed that WSS has an impact on proinflammatory pathways, extracellular matrix degradation, and remodeling processes.[45-48] Our results suggest that low WSS, increased OSI, and larger low shear areas might be associated with AWE, in accordance to a recently published study.[49] However, none of the investigated hemodynamic parameters reached significance, which could have been caused by the small sample size. Nevertheless, there was a tendency of F low toward significance, which may indicate that there is an overall association between AWE and low WSS.

Limitations and Generalizability

This study is limited by its small sample size. We included only patients with UIAs; the additional comparison of the ruptured vs unruptured IAs with regard to the parameters investigated here might increase the understanding of the role of inflammation in the natural course of IAs. The investigation of a defined number of IMs in this study represents a selection bias. We acknowledge that the focal AWE at the inner face of the aneurysm wall could be an artificial reflection of changes in the blood flow (slow flow and low WSS); however, these flow conditions are well known to induce inflammation.[50] In addition, the design of this study did not focus on the longitudinal collection of patient data, which is why no conclusion can be drawn about the influence of aneurysm growth on the results presented here. With regard to the statistics, it must be noted that there is a risk for type I errors because of the small sample size and comparatively large number of investigated parameters. The application of multivariate analysis in future studies with a larger patient cohort is therefore needed.

However, adequate data were obtained to demonstrate the associations between AWE, morphological and hemodynamic characteristics, and intrasaccular plasma concentrations of IMs. We performed an extensive analysis, which is a promising approach toward the establishment of AWE as a reliable surrogate of aneurysm stability. Future studies should consider the additional performance of histological examinations and the implementation of multicenter cooperation.

CONCLUSION

Enhancing aneurysms have large diameters and show irregular shapes. UIAs with low AWE have small diameters and are more regularly shaped. Low shear force occurring on the aneurysm area under low AWE could indicate aneurysm instability. The high plasma concentration of the anti-inflammatory cytokine IL-10 in the lumen of UIA might be associated with the prevention of cell damage and reduction of the occurrence of arteriosclerosis, which supports the hypothesis that nonenhancing UIA should rather be considered as stable rather than unstable. In addition, these results suggest that inflammation in aneurysm walls might be T

cell modulated. Therefore, AWE shows associations with established indicators of aneurysm instability.

Funding

This study was funded by an NIH-R01-Grant (grant number NS107293) granted to Dr Hasan; the 2019 Bee Foundation Aneurysm Research Grant and the Society of Vascular and Interventional Neurology Grant were both granted to Dr Samaniego. In addition, this study was partly funded by the Federal Ministry of Education and Research (grant number 13GW0473A) and the German Research Foundation (grant numbers SA 3461/2-1 and BE 6230/2-1).

Disclosures

The authors have no personal, financial, or institutional interest in any of the drugs, materials, or devices described in this article. Dr Samaniego is a consultant for Medtronic and MicroVention.

REFERENCES

1. Vlak MH, Algra A, Brandenburg R, Rinkel GJ. Prevalence of unruptured intracranial aneurysms, with emphasis on sex, age, comorbidity, country, and time period: a systematic review and meta-analysis. *Lancet Neurol*. 2011;10(7):626-636.
2. Gabriel RA, Kim H, Sidney S, et al. Ten-year detection rate of brain arteriovenous malformations in a large, multiethnic, defined population. *Stroke*. 2010;41(1):21-26.
3. Samaniego EA, Roa JA, Hasan D. Vessel wall imaging in intracranial aneurysms. *J Neurointerv Surg*. 2019;11(11):1105-1112.
4. Texakalidis P, Hilditch CA, Lehman V, Lanzino G, Pereira VM, Brinjikji W. Vessel wall imaging of intracranial aneurysms: systematic review and meta-analysis. *World Neurosurg*. 2018;117:453-458.e1.
5. Roa JA, Zanaty M, Piscopo AJ, et al. Contrast enhancement of brain aneurysms on high-resolution vessel wall imaging [HR-VWI] correlates with the presence of microbleeds. *Cardiol Cardiovasc Med*. 2021;5(1):162-171.
6. Roa JA, Zanaty M, Osorno-Cruz C, et al. Objective quantification of contrast enhancement of unruptured intracranial aneurysms: a high-resolution vessel wall imaging validation study [published online ahead of print: February 7, 2020]. *J Neurosurg*. doi:10.3171/2019.12.JNS192746.
7. Roa JA, Zanaty M, Ishii D, et al. Decreased contrast enhancement on high-resolution vessel wall imaging of unruptured intracranial aneurysms in patients taking aspirin [published online ahead of print: March 6, 2020]. *J Neurosurg*. doi:10.3171/2019.12.JNS193023.
8. Omodaka S, Endo H, Niizuma K, et al. Quantitative assessment of circumferential enhancement along the wall of cerebral aneurysms using MR imaging. *AJNR Am J Neuroradiol*. 2016;37(7):1262-1266.
9. Chalouhi N, Points L, Pierce GL, Ballas Z, Jabbour P, Hasan D. Localized increase of chemokines in the lumen of human cerebral aneurysms. *Stroke*. 2013;44(9):2594-2597.
10. Nakagawa D, Zanaty M, Hudson J, et al. Plasma soluble human elastin fragments as an intra-aneurysmal localized biomarker for ruptured intracranial aneurysm. *J Am Heart Assoc*. 2018;7(17):e010051.
11. Chalouhi N, Jabbour P, Zanaty M, et al. Sex differential in 15-hydroxyprostaglandin dehydrogenase levels in the lumen of human intracranial aneurysms. *J Am Heart Assoc*. 2017;6(10):e006639.
12. Berg P, Saalfeld S, Voß S, et al. Does the DSA reconstruction kernel affect hemodynamic predictions in intracranial aneurysms? An analysis of geometry and blood flow variations. *J Neurointerv Surg*. 2018;10(3):290-296.
13. Glaßer S, Berg P, Neugebauer M, Preim B. Reconstruction of 3D surface meshes for blood flow simulations of intracranial aneurysms. Paper presented at: Proceedings of the Conference of the German Society for Computer and Robotic Assisted Surgery 2015.
14. Saalfeld S, Berg P, Niemann A, Luz M, Preim B, Beuing O. Semiautomatic neck curve reconstruction for intracranial aneurysm rupture risk assessment based on morphological parameters. *Int J Comput Assist Radiol Surg*. 2018;13(11):1781-1793.
15. Berg P, Saalfeld S, Voß S, Beuing O, Janiga G. A review on the reliability of hemodynamic modeling in intracranial aneurysms: why computational fluid dynamics alone cannot solve the equation. *Neurosurg Focus*. 2019;47(1):E15.
16. Berg P, Stucht D, Janiga G, Beuing O, Speck O, Thévenin D. Cerebral blood flow in a healthy Circle of Willis and two intracranial aneurysms: computational fluid dynamics versus four-dimensional phase-contrast magnetic resonance imaging. *J Biomech Eng*. 2014;136(4):041003.
17. Chnafa C, Brina O, Pereira VM, Steinman DA. Better than nothing: a rational approach for minimizing the impact of outflow strategy on cerebrovascular simulations. *AJNR Am J Neuroradiol*. 2018;39(2):337-343.
18. Cebral JR, Mut F, Weir J, Putman C. Quantitative characterization of the hemodynamic environment in ruptured and unruptured brain aneurysms. *AJNR Am J Neuroradiol*. 2011;32(1):145-151.
19. Chalouhi N, Ali MS, Jabbour PM, et al. Biology of intracranial aneurysms: role of inflammation. *J Cereb Blood Flow Metab*. 2012;32(9):1659-1676.
20. Hasan D, Chalouhi N, Jabbour P, Hashimoto T. Macrophage imbalance (M1 vs. M2) and upregulation of mast cells in wall of ruptured human cerebral aneurysms: preliminary results. *J Neuroinflammation*. 2012;9:222.
21. Chyatte D, Bruno G, Desai S, Todor DR. Inflammation and intracranial aneurysms. *Neurosurgery*. 1999;45(5):1137-1146; discussion 1146-1147.
22. Tulamo R, Frösen J, Hernesniemi J, Niemelä M. Inflammatory changes in the aneurysm wall: a review. *J Neurointerv Surg*. 2018;10(Suppl 1):i58-i67.
23. Wynn TA. Cellular and molecular mechanisms of fibrosis. *J Pathol*. 2008;214(2):199-210.
24. Crompton MR. Mechanism of growth and rupture in cerebral berry aneurysms. *Br Med J*. 1966;1(5496):1138-1142.
25. Frösen J, Piippo A, Paetau A, et al. Remodeling of saccular cerebral artery aneurysm wall is associated with rupture: histological analysis of 24 unruptured and 42 ruptured cases. *Stroke*. 2004;35(10):2287-2293.
26. Aoki T, Kataoka H, Ishibashi R, Nozaki K, Egashira K, Hashimoto N. Impact of monocyte chemoattractant protein-1 deficiency on cerebral aneurysm formation. *Stroke*. 2009;40(3):942-951.
27. Starke RM, Chalouhi N, Jabbour PM, et al. Critical role of TNF-α in cerebral aneurysm formation and progression to rupture. *J Neuroinflammation*. 2014;11:77.
28. Ali MS, Starke RM, Jabbour P, et al. 184 infliximab suppresses TNF-α induced inflammatory phenotype in cerebral vascular smooth muscle cells: implications for cerebral aneurysm formation. *Neurosurgery*. 2013;60:181.
29. Moriwaki T, Takagi Y, Sadamasa N, Aoki T, Nozaki K, Hashimoto N. Impaired progression of cerebral aneurysms in interleukin-1beta-deficient mice. *Stroke*. 2006;37(3):900-905.
30. Borish LC, Steinke JW. 2. Cytokines and chemokines. *J Allergy Clin Immunol*. 2003;111(2):S460-S475.
31. Ou H, Guo B, Liu Q, et al. Regulatory T cells as a new therapeutic target for atherosclerosis. *Acta Pharmacol Sin*. 2018;39(8):1249-1258.
32. Potteaux S, Esposito B, van Oostrom O, et al. Leukocyte-derived interleukin 10 is required for protection against atherosclerosis in low-density lipoprotein receptor knockout mice. *Arterioscler Thromb Vasc Biol*. 2004;24(8):1474-1478.
33. Mallat Z, Gojova A, Brun V, et al. Induction of a regulatory T cell type 1 response reduces the development of atherosclerosis in apolipoprotein E-knockout mice. *Circulation*. 2003;108(10):1232-1237.
34. Backes D, Hendrikse J, van der Schaaf I, et al. Determinants of gadolinium-enhancement of the aneurysm wall in unruptured intracranial aneurysms. *Neurosurgery*. 2018;83(4):719-725.
35. Lv N, Karmonik C, Chen S, et al. Relationship between aneurysm wall enhancement in vessel wall magnetic resonance imaging and rupture risk of unruptured intracranial aneurysms. *Neurosurgery*. 2019;84(6):E385-E391.
36. Wang G-X, Li W, Lei S, Ge X-D, Yin J-B, Zhang D. Relationships between aneurysmal wall enhancement and conventional risk factors in patients with intracranial aneurysm: a high-resolution MRI study. *J Neuroradiol*. 2019;46(1):25-28.
37. International Study of Unruptured Intracranial Aneurysms Investigators. Unruptured intracranial aneurysms–risk of rupture and risks of surgical intervention. *N Engl J Med*. 1998;339(24):1725-1733.
38. Wiebers DO, Whisnant JP, Huston J, et al. Unruptured intracranial aneurysms: natural history, clinical outcome, and risks of surgical and endovascular treatment. *Lancet*. 2003;362(9378):103-110.
39. Juvela S, Porras M, Poussa K. Natural history of unruptured intracranial aneurysms: probability of and risk factors for aneurysm rupture. *J Neurosurg*. 2008;108(5):1052-1060.
40. Kleinloog R, de Mul N, Verweij BH, Post JA, Rinkel GJE, Ruigrok YM. Risk factors for intracranial aneurysm rupture: a systematic review. *Neurosurgery*. 2018;82(4):431-440.

41. Raghavan ML, Ma B, Harbaugh RE. Quantified aneurysm shape and rupture risk. *J Neurosurg*. 2005;102(2):355-362.
42. Tremmel M, Dhar S, Levy EI, Mocco J, Meng H. Influence of intracranial aneurysm-to-parent vessel size ratio on hemodynamics and implication for rupture: results from a virtual experimental study. *Neurosurgery*. 2009;64(4):622-630; discussion 630-631.
43. Xiang J, Natarajan SK, Tremmel M, et al. Hemodynamic-morphologic discriminants for intracranial aneurysm rupture. *Stroke*. 2011;42(1):144-152.
44. Xiang J, Tutino VM, Snyder KV, Meng H. CFD: computational fluid dynamics or confounding factor dissemination? The role of hemodynamics in intracranial aneurysm rupture risk assessment. *AJNR Am J Neuroradiol*. 2014;35(10):1849-1857.
45. Metaxa E, Tremmel M, Natarajan SK, et al. Characterization of critical hemodynamics contributing to aneurysmal remodeling at the basilar terminus in a rabbit model. *Stroke*. 2010;41(8):1774-1782.
46. Malek AM, Alper SL, Izumo S. Hemodynamic shear stress and its role in atherosclerosis. *JAMA*. 1999;282(21):2035-2042.
47. Kolega J, Gao L, Mandelbaum M, et al. Cellular and molecular responses of the basilar terminus to hemodynamics during intracranial aneurysm initiation in a rabbit model. *J Vasc Res*. 2011;48(5):429-442.
48. Wang Z, Kolega J, Hoi Y, et al. Molecular alterations associated with aneurysmal remodeling are localized in the high hemodynamic stress region of a created carotid bifurcation. *Neurosurgery*. 2009;65(1):169-177; discussion 177-178.
49. Larsen N, Flüh C, Saalfeld S, et al. Multimodal validation of focal enhancement in intracranial aneurysms as a surrogate marker for aneurysm instability. *Neuroradiology*. 2020;62(12):1627-1635.
50. Boussel L, Rayz V, McCulloch C, et al. Aneurysm growth occurs at region of low wall shear stress: patient-specific correlation of hemodynamics and growth in a longitudinal study. *Stroke*. 2008;39(11):2997-3002.

Supplemental digital content *is available for this article at www.neurosurgery-online.com.*

Supplemental Digital Content. Table. Measured values of morphological and hemodynamic parameters and inflammatory mediators. The table presented here indicates the absolute values of the investigated morphological and hemodynamic parameters as well as the inflammatory mediators. In addition, the demographic data of the patients and the measured values of the CR_{stalk} are listed. We excluded one aneurysm from the morphological and hemodynamic analysis because of failure during the neck reconstruction occurred and 5 aneurysms from the blood sample analysis due to hemolyzed samples.